

Modeling urban growth using spatially heterogeneous cellular automata models: Comparison of spatial lag, spatial error and GWR



Chen Gao^{a,b}, Yongjiu Feng^{b,c,✉*}, Xiaohua Tong^{b,*}, Zhenkun Lei^a, Shurui Chen^a, Shuting Zhai^a

^a College of Marine Sciences, Shanghai Ocean University, Shanghai 201306, China

^b College of Surveying & Geo-Informatics, and The State Key Laboratory of Disaster Reduction in Civil Engineering, Tongji University, Shanghai 200092, China

^c College of Architecture & Urban Planning, Tongji University, Shanghai 200092, China

ARTICLE INFO

Keywords:

Urban growth modeling
Transition rules
Spatial regression
Spatial heterogeneity
Figure-of-merit
Nanjing

ABSTRACT

Many methods can be used to construct geographical cellular automata (CA) models of urban land use, but most do not adequately capture spatial heterogeneity in urban dynamics. Spatial regression is particularly appropriate to address the problem to reproduce urban patterns. To examine the advantages and disadvantages of spatial regression, we compare a spatial lag CA model (SLM-CA), a spatial error CA model (SEM-CA) and a geographically-weighted regression CA model (GWR-CA) by simulating urban growth at Nanjing, China. Each CA model is calibrated from 1995 to 2005 and validated from 2005 to 2015. Among these, SLM and SEM are spatial autoregressive (SAR) models that consider spatial autocorrelation of urban growth and yield highly similar land transition probability maps. Both SAR-CA and GWR-CA accurately reproduce urban growth at Nanjing during the calibration and validation phases, yielding overall accuracies (OAs) exceeding 94% and 85%, respectively. SAR-CA is superior in simulating urban growth when measured by OA and figure-of-merit (FOM) while GWR-CA is superior regarding the ability to address spatial heterogeneity. A concentric ring buffer-based assessment shows OA valleys that correspond to FOM peaks, where the ranges of valleys and peaks indicate the areas with active urban development. By comparison, SAR-CA captures more newly-urbanized patches in highly-dense urban areas and shows better performance in terms of simulation accuracy; whereas, GWR-CA captures more in the suburbs and shows better ability to address spatial heterogeneity. Our results demonstrate that spatial regression can help produce accurate simulations of urban dynamics featured by spatial heterogeneity, either implicitly or explicitly. Our work should help select appropriate CA models of urban growth in different terrain and socioeconomic contexts.

1. Introduction

Spatial heterogeneity refers to non-uniformity and complexity in the distribution of land use patterns. Land use change is a spatially varying human-induced process that promotes urbanization and substantially affects the natural environment (Lambin & Meyfroidt, 2011; Liu et al., 2017; Pinto, Antunes, & Roca, 2017) where spatial heterogeneity can yield different results of land use dynamics at different observation positions (Feng & Tong, 2018; Kassawmar, Eckert, Hurni, Zeleke, & Hurni, 2016; Valipour, 2014; Yi et al., 2018). Rapid urban growth in turn leads to increasingly fragmented landscapes characterized by enhanced spatial heterogeneity (Irwin, 2010). Accordingly, it is essential to characterize landscape heterogeneity properly and incorporate it into land use models to achieve better predictions of future scenarios in

support of planning and decision-making (Debonne, van Vliet, Heinemann, & Verburg, 2018; Tang et al., 2018).

Cellular automata (CA) are well-known self-organizing models for simulating the dynamics and future scenarios in geographical systems (Dragičević, 2010; Lai, Dragičević, & Schmidt, 2013). CA models are usually comprised of five essential components: tessellated cells, finite cell states, cell neighborhoods, randomness, and global drivers (Batty, Xie, & Sun, 1999; Couclelis, 1997; Tobler, 1970; Von Neumann & Burks, 1966; White & Engelen, 1993). Among these, cell states are determined using CA transition rules defined by the relationships between the dynamics and their drivers (Clarke, 2018; Kocabas & Dragicevic, 2007; Phipps, 2018). Geographical CA are self-producing and spatial approaches, which are usually integrated with geographical information systems (GIS) to improve their ability of spatial computation and

* Corresponding author.

** Corresponding author at: College of Surveying & Geo-Informatics, The State Key Laboratory of Disaster Reduction in Civil Engineering, Tongji University, Shanghai 200092, China.

E-mail addresses: yjfeng@tongji.edu.cn (Y. Feng), xhtong@tongji.edu.cn (X. Tong).

heterogeneity identification (Abdullahi & Pradhan, 2018; Guan, Shi, Huang, & Lai, 2016). These features have made CA modeling the preferred method of spatially-explicit simulation in recent decades (Alexandridis, Russo, Vakalis, Bafas, & Siettos, 2011), where modeling urban growth is the most typical application (Hewitt & Diaz-Pacheco, 2017; Liu et al., 2017; Mustafa et al., 2018; Wu et al., 2019).

Earlier studies applied many different methods such as statistical approaches and intelligent algorithms to retrieve CA transition rules for calculating land use transition probabilities. Typical methods are non-spatial statistics such as logistic regression (LR), partial least squares regression, generalized additive models, and principal component analysis (Arsanjani, Helbich, Kainz, & Boloorani, 2013; Gashaw, Tulu, Argaw, & Worqlul, 2018; Wang et al., 2016), as well as spatial statistics such as spatial autoregressive (SAR) and geographic weighted regression (GWR) (Feng & Tong, 2018; Feng, Yang, Hong, & Cui, 2018; Ku, 2016; Mirbagheri & Alimohammadi, 2017). Intelligent algorithms include machine learning approaches such as artificial neural network and deep learning (Shafizadeh-Moghadam, 2019; Zhao, Chen, Wu, Chen, & Liu, 2017), as well as heuristic algorithms such as genetic algorithm (GA), particle swarm optimization (PSO), simulated annealing, and differential evolution (Gholizadeh, 2013; Ma, He, Liu, & Yu, 2011). Non-spatial statistical methods and intelligent algorithms have limitations in explicitly capturing spatial heterogeneity in the landscape when they use only a single set of CA parameters for modeling urban growth (Shafizadeh-Moghadam, 2019; White & Engelen, 1997; Wu, 2002). In fact, a driving factor may promote urban growth at a position but inhibit urban growth at another position (Feng & Tong, 2018; Mirbagheri & Alimohammadi, 2017). A recent publication (Mustafa, Ebaid, & Teller, 2018) shows that GA can find multiple solutions to model spatial heterogeneity in the relationships between urban dynamics and their drivers, where each solution (i.e. a set of CA parameters) is suitable for specific locations across the study area.

In CA modeling, spatial heterogeneity can be delineated by heterogeneous neighborhoods and/or spatially varying transition rules (Feng & Tong, 2018; Ku, 2016; Moreno, Wang, & Marceau, 2009). Concerning the neighborhood configuration, the modeling space can be divided into irregular shapes for simulating land use patterns, where each shape has a different, asynchronous size (Moreno et al., 2009). Also, a region-partition method constructs a unique CA model in each sub-region to capture spatial heterogeneity (Triantakonstantis, Mountrakis, & Wang, 2011). Recently, Feng and Tong (2019a) applied land use gradient and land use hotspots to define heterogeneous neighborhood configuration of CA models, incorporating landscape heterogeneity that eventually leads to accurate simulations of urban growth in rapidly-developing areas. These studies of heterogeneous neighborhoods enhanced our knowledge of spatially-varying interactions among nearby cells. However, defining transition rules considering spatial heterogeneity is very important for CA-based urban growth modeling because these rules lie at the models.

Spatial regression is a particularly appropriate method for delineating spatial heterogeneity because the method incorporates the locations of urban growth and its drivers to characterize their changes across space (Feng et al., 2018; Gao, Zhang, He, & Liu, 2017; Ku, 2016; Mirbagheri & Alimohammadi, 2017). Similar to non-spatial methods (e.g. LR), spatial regression produces CA parameters with clear physical meanings that represent the impact of each driving factor of urban growth. Specifically, spatial regression considers either the spatial autocorrelation among nearby cells or the location of each observation. SAR and GWR are typical spatial regression methods that have been applied to the analysis and modeling of urban land use change. Representative SAR methods include the spatial lag model (SLM) and the spatial error model (SEM). Each considers the spatial autocorrelation among observations to reduce the spatial clustering in model residuals (Feng et al., 2018; Ku, 2016). As such, SAR implicitly addresses spatial heterogeneity to produce better CA transition rules. In comparison, GWR explicitly addresses spatial heterogeneity by producing position-

based CA parameters. It considers local features and takes into account the influence of locations (Gao et al., 2017; Mirbagheri & Alimohammadi, 2017). Feng and Tong (2018) proposed a novel CA model (GWR-CA) based on GWR to simulate urban land use change at Suzhou from 2000 to 2015. In GWR-CA, each driving factor contains effects that both promote and resist urban land use change, explicitly depicting the complexity and heterogeneity in urban growth. Although both SAR and GWR are spatial regression methods, their mechanisms differ when solving spatial heterogeneity. This study aims to compare SAR and GWR in constructing CA models, thus identifying their pros and cons for dynamic urban growth simulation.

Here, we develop three CA models using SLM, SEM and GWR to simulate dynamic urban growth at Nanjing from 1995 to 2015. Typically, the proposed CA models are calibrated from the initial time (T0) to the final time (T1), and then validated by predicting urban growth to a future time (T2) (Tong & Feng, 2019b; van Vliet, Bregt, & Hagen-Zanker, 2011). Following this definition, we first calibrated the SLM-CA, SEM-CA and GWR-CA models using the 1995–2005 historical urban land use, and then validated these models using the 2005–2015 historical urban land use. Overall accuracy (OA) and figure-of-merit (FOM) were used to evaluate the simulation and prediction results.

2. Spatially heterogeneous CA models

2.1. CA modeling approach

The modeling procedure has three steps: training, calibration, and validation (Fig. 1). The training step incorporates urban pattern mapping, driving factor production, sample selection, transition retrieval, and model component definition. The calibration step consists of model parameter adjustment, urban pattern simulation for the calibration phase, and result assessment. The validation step includes scenario prediction for the validation phase and result assessment. We applied the UrbanCA software (Feng & Tong, 2019b) to construct the CA models based on spatial lag, spatial error and GWR as well as compare their simulation results.

CA transition rules represent the combined effects of the present cell state (*Sta.p*), the partial transition probability defined by global drivers (*P.v*), the local neighborhood effect (*N.e*), the global and local constraints (*Con*), and a stochastic factor (*Sto*). The global transition probability (*P_{all}*) and the decision rules can be given by (Rimal et al., 2018; Wu, 2002):

$$\left\{ \begin{array}{l} \text{Probability: } P_{all} \sim P(\text{UrbanCARule}(\text{Sta. } p, P.v, N.e, Con, Sto)) \\ \text{Decision: Sta. } n = \text{Urban if } P_{all} \geq P_{th} \\ \text{Decision: Sta. } n = \text{Nochange if } P_{all} < P_{th} \end{array} \right. \quad (1)$$

where *UrbanCARule* denotes the transition function, *Sta.n* denotes cell state at the next time step, and *P_{th}* denotes a predefined threshold. The global probability is compared with the threshold to define the decision rules.

Although many modelers multiplied all the terms in Eq. (1) to compute the global transition probability, the sum of the terms was also considered justifiable in urban growth modeling (White & Engelen, 1993, 1997). A most recent publication has further justified the additive operation (Feng & Tong, 2019b). Here, we use the sum of transition probability and neighborhood effect to help calculate the global transition probability. In CA models, many publications incorporated a stochastic term to simulate uncertainties caused by unknown disturbances and policy changes (Mustafa, Saadi, Cools, & Teller, 2018; Vermeiren, Vanmaercke, Beckers, & Van Rompaey, 2016; White & Engelen, 1993), while some other did not include such a term (Mustafa, Rienow, Saadi, Cools, & Teller, 2018; Omrani, Tayyebi, & Pijanowski, 2017). Because an error item has been included in the driver-based partial transition probability, we do not introduce the stochastic factor in calculating the global probability. Thereby, the global probability

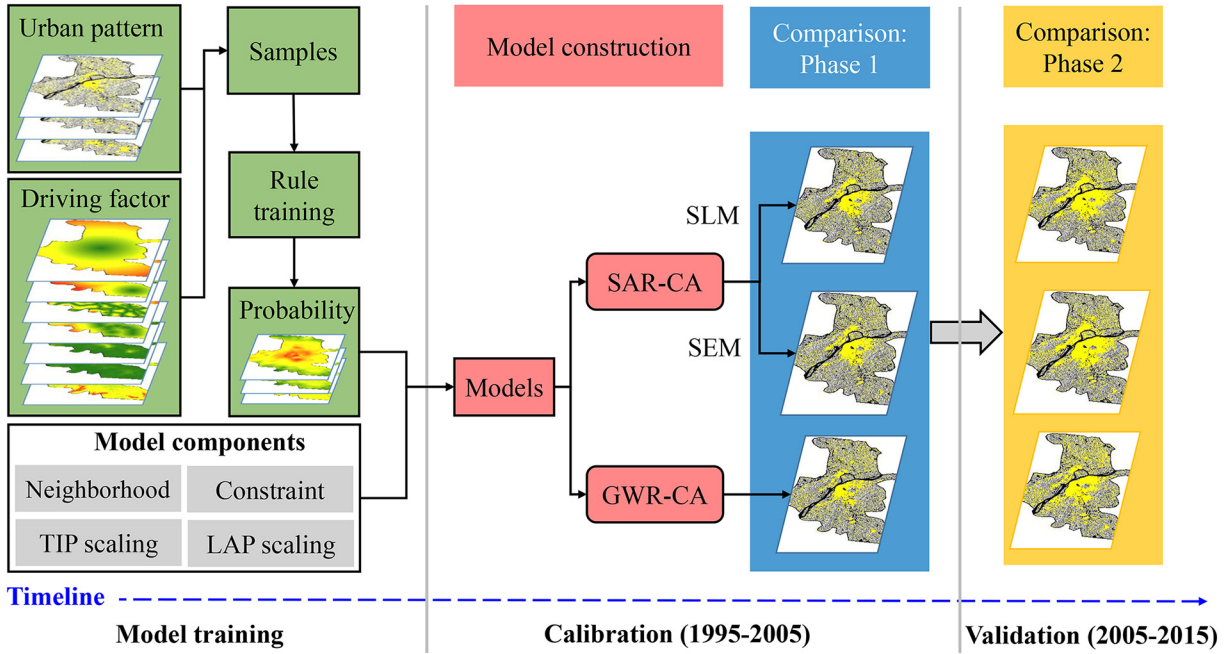


Fig. 1. Procedure for modeling dynamic urban growth using heterogeneous CA models.

can be given by:

$$P_{all} = (P.v \cdot (1 + TIP)^{t-1} + N.e \cdot LAP) \cdot \frac{Con}{2} \quad (2)$$

where *TIP* is a scaling parameter that compensates for the decaying effect of the partial probability (*P.v*), and *LAP* is a scaling parameter that offsets the increasing neighborhood effect (*N.e*). According to the UrbanCA software, *TIP* ranges from 0.00 to 0.05 where a larger value denotes a stronger effect, and *LAP* ranges from 0.5 to 1.0 where a smaller value denotes a weaker effect (Feng & Tong, 2019b). These authors assigned 0.01 for *TIP* and 0.8 for *LAP* as default parameters after extensive case-based testing. We then followed Feng and Tong (2019b) to use the default parameters in our CA models.

The partial transition probability (*P.v*) is calculated considering independent variables \mathbf{x} (i.e. urban growth drivers), a dependent variable y (i.e. urban land use change), and the modeling errors ϵ . The partial probability can be given by (Wu, 2002; Phipps, 2018):

$$\begin{aligned} P.v(\alpha_0, \mathbf{a}) &= \frac{\exp(\alpha_0 + \mathbf{a} \cdot \mathbf{x} + by + \epsilon)}{1 + \exp(\alpha_0 + \mathbf{a} \cdot \mathbf{x} + by + \epsilon)} \\ &= \frac{\exp((\sum_{i=0}^n a_i x_i) + by + \epsilon)}{1 + \exp((\sum_{i=0}^n a_i x_i) + by + \epsilon)} \end{aligned} \quad (3)$$

where α_0 denotes a constant, $\mathbf{a} [= (a_1, \dots, a_n)]$ denotes the weights of the independent variables (x_1, \dots, x_n), and x_0 equals 1. Also, b is the weight of the dependent variable if an autoregressive model is applied, where $b = 0$ if y is not included in the calculation.

The neighborhood effect is a representation of CA self-organization, reflecting the essential "bottom-to-top" approach of individual models (Pérez-Molina, Sliuzas, Flacke, & Jetten, 2017). The neighborhood effect is usually defined using a regular window (Moreno et al., 2009):

$$N.e = \frac{\sum_{j=1}^m \text{Binarization}(Sta}_j = \text{Urban})_t}{m} \quad (4)$$

where $m [= (\text{row} \times \text{col}-1)]$ is the number of cells in the neighborhood (window). *Binarization(.)* is a conditional function that returns 1 if the present cell state Sta_j is urban; otherwise, it returns 0.

The CA state transition is also restricted by global and local conditions. The global constraint denotes the total demand of new urban space while the local constraint denotes the specific restrictions of

broad water bodies and protected areas. Here, we replace the corresponding items in Eq. (2) using the transition probability in Eq. (3) and the neighborhood effect in Eq. (4), and these jointly compute the global transition probability.

2.2. The SAR-CA model

SAR delineates the relationships between urban growth and its drivers by considering spatial autocorrelation (Ver Hoef, Peterson, Hooten, Hanks, & Fortin, 2018). It is a position-based statistical member of the linear regression family, and can implicitly address spatial heterogeneity in geographic phenomena, reducing the spatial clustering in modeling residuals (Anselin, 2016). As a typical SAR, SLM shows that the dependent variable Y is not only related to the independent variable X , but also related to the dependent variable in neighboring regions (Conway, Li, Wolch, Kahle, & Jerrett, 2008). The SLM can be defined as (Mur & Angulo, 2006):

$$\begin{cases} Y = \alpha_0 + X\mathbf{a} + \rho WY + \epsilon \\ w_{pq} = \begin{cases} d_{pq}, & \text{if cell } p \text{ is adjacent to cell } q \\ 0, & \text{if cell } p \text{ is not adjacent to cell } q \end{cases} \\ \epsilon \sim N(0, \sigma^2 I_n) \end{cases} \quad (5)$$

where ρ denotes the coefficient of spatial lag (Wy); W denotes the standardized spatial weight matrix that allows only adjacent neighbors to affect each other, where w_{pq} is the specific weight between cell p and cell q and is an element of W ; σ^2 denotes the variance of the spatially independent error ϵ ; and I_n denotes Moran's I.

In comparison, SEM includes the spatial autocorrelation of the same independent variable among neighborhoods instead of among dependent variables. This indicates the absence of the dependence of spatial errors in SEM (Elhorst, 2010). By distinguishing the spatially dependent error μ and the spatially independent error ϵ , SEM can be represented as (Zhang, Du, Geng, Liu, & Huang, 2015):

$$\begin{cases} Y = \alpha_0 + X\mathbf{a} + \mu \\ \mu = (I - \lambda W)^{-1}\epsilon \end{cases} \quad (6)$$

where I denotes a unit vector and λ denotes the coefficient of the spatial error. Based on SLM (6) and SEM (7), the driver-based partial transition

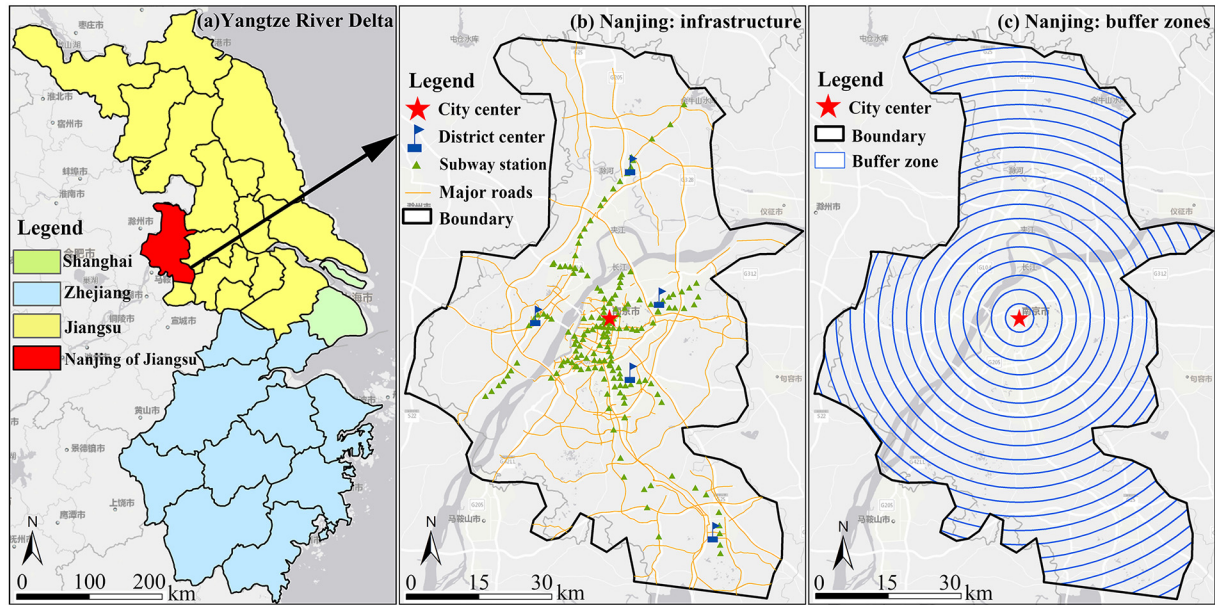


Fig. 2. The Nanjing study area: (a) Yangtze River Delta, (b) Nanjing city, and (c) buffers used to examine accuracy change.

probability can be defined by:

$$\left\{ \begin{array}{l} \text{SLM: } P.v(\alpha_0, a, \rho W) = \frac{\exp(\alpha_0 + Xa + \rho WY + \varepsilon)}{1 + \exp(\alpha_0 + Xa + \rho WY + \varepsilon)} \\ \text{SEM: } P.v(\alpha_0, a, \lambda W) = \frac{\exp(\alpha_0 + Xa + (I - \lambda W)^{-1}\varepsilon)}{1 + \exp(\alpha_0 + Xa + (I - \lambda W)^{-1}\varepsilon)} \end{array} \right. \quad (7)$$

2.3. The GWR-CA model

GWR explicitly addresses spatial heterogeneity by examining the spatial and quantitative relationships between the dependent and independent variables using spatially varying coefficients (Mirbagheri & Alimohammadi, 2017). In urban modeling, each factor in GWR both promotes and resists urban land use change (Feng & Tong, 2018). GWR can be given by (Gao & Li, 2011):

$$W_k y_k = \mathbf{a}_0(u_k, v_k) + \sum_{i=1}^n W_k \mathbf{a}_i(u_k, v_k) x_{ik} + \delta_k, \quad k = 1, \dots, m \quad (8)$$

where, for the k^{th} sample, (u_k, v_k) denotes the coordinates, \mathbf{W}_k denotes the spatial weight, $\mathbf{a}_0(u_k, v_k)$ denotes the constant vector, $\mathbf{a}_i(u_k, v_k)$ denotes the regression parameter vector, and δ_k denotes the random error vector. Samples closer to the one in regressing have greater impacts on parameter estimation than those further away. A distance-decay function is usually used to define the influencing weight \mathbf{W}_k . The specific weight w_{ij} between sample i and sample j can be given by (Lu, Yang, Ge, & Harris, 2018):

$$w_{ij} = \exp\left(-\frac{d_{ij}^2}{B^2}\right) \quad (9)$$

where d_{ij} denotes the distance between the two samples, and B is the bandwidth denoting the neighborhoods that affect the sample in regressing. Because GWR is sensitive to the bandwidth, which should be optimized during model construction (Su, Li, Hu, Xiao, & Zhang, 2014). Based on GWR (9), the partial transition probability based on drivers can be defined by:

$$\text{GWR: } P.v(\mathbf{a}_0, \mathbf{a}) = \frac{\exp(\mathbf{a}_0(u_k, v_k) + \sum_{i=1}^n W_k \mathbf{a}_i(u_k, v_k) x_{ik} + \delta_k)}{1 + \exp(\mathbf{a}_0(u_k, v_k) + \sum_{i=1}^n W_k \mathbf{a}_i(u_k, v_k) x_{ik} + \delta_k)} \quad (10)$$

2.4. Assessment methods

We conducted pixel-by-pixel comparison between the simulated and real results to produce an error matrix, which reports assessment metrics such as OA and Kappa coefficients (Fung & Le Drew, 1988; Tong & Feng, 2019b). OA indicates the overall agreement between the simulated and real end-states, which incorporate a large proportion of state-persistent cells. To assess the state change, five other metrics were derived by overlaying three maps: the start real map, the end real map and the simulated map. The metrics include hits, misses, false alarms, and correct rejection (Pontius & Millones, 2011), which jointly generate a new FOM metric. OA and FOM were defined as (Pontius et al., 2008):

$$\left\{ \begin{array}{l} \text{Overall accuracy} = \frac{\text{Cells on the diagonal in error matrix}}{\text{All cells}} \\ \text{Overall accuracy} = \text{Initial Urban} + \text{Correct Rejection} + \text{Hits} \\ \text{FOM} = \text{Hits}/(\text{Hits} + \text{Misses} + \text{False Alarms}) \end{array} \right. \quad (11)$$

where *Initial Urban* indicates the real urban areas at the start time, *Correct Rejection* indicates the persistent non-urban area during modeling, *Hits* indicate the real growth simulated as growth, *Misses* indicate the real growth simulated as persistent non-urban, and *False Alarms* indicate the real persistent non-urban simulated as growth. A larger OA indicates a higher overall agreement between the simulated and real results, while a larger FOM indicates a better ability of the model to capture urban growth.

3. Case study area

3.1. Study area and the observed land change

Our Nanjing case study area is one of the most important gateway cities located in the lower reaches of the Yangtze River Delta (Fig. 2a). Nanjing comprises 11 districts with a total area of 6587 km² (Shu et al., 2017). It has a forest-coverage rate of ~30% in the study area and a vegetation-coverage rate of ~45% in the built-up area (Dong, Dai, Shao, & Xu, 2015). The superior geographical position of Nanjing has made it an essential waypoint on the route between Beijing and Shanghai. Nanjing is now a national transport hub with high-level transport networks of road, train and air, and the network density is top-ranking among Chinese cities (Zhang, Hu, Chen, & Xu, 2012). The city also has sophisticated subway systems with 378 km of track and

174 stations (Fig. 2b). As of 2017, there were a total of 8.3 million registered residents, of which 81% were urban residents (Nanjing Municipal Bureau Statistics, 2015). Gross domestic product (GDP) in Nanjing has increased from 3.4 billion Chinese Yuan (~500 million USD) to 960 billion Chinese Yuan (~140 billion USD) over the past 40 years (Qiao et al., 2017). Infrastructure improvement, population growth and economic prosperity have led to high demand for commercial and living space, resulting in rapid growth of built-up area (Huang, Li, Zhao, & Zhu, 2008).

Therefore, Nanjing is of great interest to modelers and scientists who wish to test their models and approaches (Cao, Bennett, Shen, & Xu, 2016; Luo & Wei, 2009; Shu et al., 2017). Here, we select Nanjing as our case study area to examine the advantages and disadvantages of the spatially heterogeneous CA models. To evaluate accuracy change, we generated 23 buffers centered on the Nanjing City center, where the inner buffer is a circle with the radius of 3 km and the others are concentric rings with the width of 3 km (Fig. 2c).

We produced land use patterns at Nanjing using Landsat images (see also the next sub-section) based on the maximum likelihood classifier. The land use types consist of urban, non-urban and excluded area (i.e. water bodies). The post-classification assessment shows that the OAs are 98.4%, 97.7% and 98.0% for 1995, 2005 and 2015, respectively. The classification displays that urban areas at Nanjing have nearly doubled in size, increasing from 15.4% in 1995, to 19.3% in 2005, and 28.2% in 2015. We used the 1995 pattern (Fig. 3a) as the start map, the 2005 pattern (Fig. 3b) as the final map for model calibration, and the 2015 pattern (Fig. 3c) as the final map for model validation. Fig. 3 shows that the new urban areas lie principally on the south side of the Yangtze River, and the city shows different urban growth rates and built-up intensities in different directions. For example, regions labeled in red show faster urban growth than other regions. These clearly illustrate spatial heterogeneity in urban land use change at Nanjing. This suggests that the drivers possess different impacts on urban growth at different positions, and the spatial heterogeneity can be explored using spatial autocorrelation inherent in SAR and spatially varying coefficients in GWR (Feng & Tong, 2018; Ku, 2016; Mirbagheri & Alimohammadi, 2017). While intelligent algorithms such as GA and PSO are featured by multiple solutions for scenario predictions under complex constraints (Mustafa, Ebaid, & Teller, 2018; Tong & Feng,

2019a), they have limitations in searching for location-based solutions to address the spatial autocorrelation and varying coefficients directly.

3.2. Datasets and input variables

We applied four raw datasets (Table 1) to produce urban pattern maps and driver maps as input to the spatially heterogeneous CA models. Geospatial Data Clouds (<http://www.gscloud.cn>) provides Landsat images for land use classification and SRTM data for terrain assessment. Policy datasets include population density assembled from Worldpop (worldpop.org.uk) and GDP assembled from NOAA national centers for environmental information (www.ngdc.noaa.gov). The infrastructure datasets from OpenStreetMap (<https://www.openstreetmap.org>) include maps of road and subway networks. The administrative maps were collected from the Geographical Information Monitoring Cloud Platform (<http://www.dsac.cn>).

To calibrate and validate the CA models, we used three inputs (Table 2): land patterns, driving factors and model components. 1) Land patterns. Land1, Land2 and Land3 are observed land use patterns for 1995, 2005 and 2015, respectively. The dependent variable is the change between Land1 and Land2, where we used "1" to denote state change and "0" to denote state persistence. 2) Driving factors. Four proximity factors include D-city, D-district, D-road and D-subway. These reflect the effects of administrative centers, infrastructure, two socioeconomic factors of macro-policy, and one biophysical factor of topographic features. 3) Model components. Neighborhood configuration is a typical model component usually defined using square, annulus, circular, irregular, or user-defined shapes. We followed a recent publication that tests the neighborhood sensitivity to select the Moore's 5×5 square neighborhoods (Zaitsev, 2017). The threshold is preferred if it results in urban cells approximating the total available cells at the maximum iterations allowed.

We produced the proximity maps using Euclidean Distance, where a low value is usually found near centers, roads, and stations (Fig. 4a-d). A non-urban cell with smaller proximity is more likely to be transformed into an urbanized cell. The POP and GDP maps are density-based, where a large value is usually found near highly urbanized areas (Fig. 4e-f). A non-urban cell with a larger POP or GDP has a greater possibility of transforming into an urbanized cell. In our study area, the

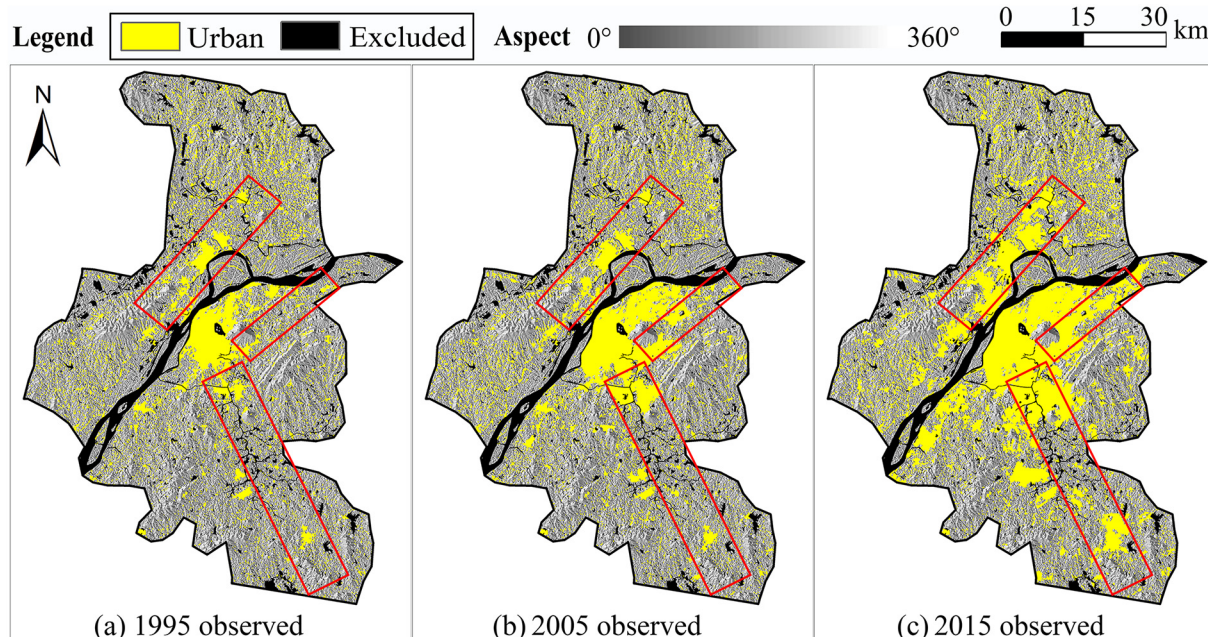


Fig. 3. Observed urban patterns for 1995, 2005 and 2015 overlaid on a terrain aspect map.

Table 1

Spatial datasets used to construct the spatially heterogeneous CA models.

Type	Dataset	Scale	Date	Use
Land	Landsat-5 TM	30 m	1995-11-21	Classify the satellite imagery to produce land use patterns for model calibration and validation
	Landsat-5 TM	30 m	2005-10-24	
	Landsat-8 OLI	30 m	2015-11-28	
Terrain	SRTM DEM V4	90 m	2008-11-25	Discern elevation of the study area
	Population density	100 m	2015	Discern total population per pixel
Policy	Gross domestic product	1000 m	2005 and 2015	Discern total GDP per pixel
	Administration	1:1000	1995–2015	Discern study boundary and social affair centers
	Transportation	1:1000	2005 and 2015	Discern arterial roads and highways
Infrastructure	Subway	1:1000	2005 and 2015	Discern subway lines and stations

Table 2

Land use patterns, driving factors and model components in the spatially heterogeneous CA models.

Category	Variable	Type	Use
Land pattern	Land1	State	Initial land use state for model calibration
	Land2	State	Final land use state for model calibration
	Land3	State	Final land use state for model validation
Driving factor	Land2 - Land1	Dependent	Differences between the initial state and the final state
	D-city	Independent	Proximity to Nanjing City center (1995–2015)
	D-district	Independent	Proximity to district centers (1995–2015)
	D-road	Independent	Proximity to arterial roads and highways (2005 and 2015)
	D-subway	Independent	Proximity to subway stations (2005 and 2015)
	POP	Independent	Reflect the effect of population density (i.e. the original POP for 2015, and the POP for 2005 calculated using the 2015 POP and the 2005 urban intensity)
	GDP	Independent	Reflect the effect of economic density (i.e. the original GDP for 2015, and the GDP for 2005 calculated using the 2015 GDP and the 2005 urban intensity)
Model component	Elevation	Independent	Reflect the effect of topography
	Neighborhood	Local	The transition potential determined by neighborhoods
	Neighborhood scaling	Local	The parameter (LAP) to modify the neighborhood effect
	Probability scaling	Global	The parameter (TIP) to modify the probability effect
	Global constraint	Global	The total urban cells available for development
	Spatial constraint	Local	Constricts for urban development at specific locations
	Threshold	Global	The uniform probability to define the decision rule

elevation and slope are highly correlated because regions with higher elevations show greater slopes; as a result, the elevation sufficiently indicates the terrain's suitability for urban development, where a smaller value suggests a higher possibility of the nonurban-to-urban transformation. Systematic sampling approach was applied to select samples from these variable maps to train the transition rules for building the CA models.

4. Results

4.1. Transition rules and model calibration

The Akaike information criterion (AIC; -724.09) for SLM is slightly smaller than that for SEM (-723.65), showing briefly better performance of the former. The parameters of SLM are between -0.16 to 0.17 and those of SEM are between -0.17 to 0.19 , denoting no significant differences between the parameter ranges. Table 3 shows that GDP is the most influential factor of urban growth, followed by elevation and D-city.

GWR is substantially affected by its bandwidth. There is an improvement of the goodness-of-fit of the transition rules when the bandwidth decreases from 1000 to 50. The GWR parameters range from -75.89 to 70.29 that demonstrates significant variation across space. Each driver yields opposing effects that both advance and impede urban growth, because each has both positive and negative weights. These weights (parameters) indicate that the variable with the strongest impact on urban growth is GDP, followed by D-subway and elevation. GWR differs significantly from SLM and SEM regarding D-city, which shows stronger effects on urban growth in the latter two models.

We defined the transition rules of CA models using the above parameters, and then produced land transition probability maps for

SLM, SEM and GWR (Fig. 5, top row). The SLM and SEM yield highly similar land transition probability maps despite the substantial differences between their parameters, suggesting that they would produce similar urban patterns. The GWR transition probability shows several clusters of high values on the south side of the Yangtze River, in the southeast, and in the north. By comparison, the SLM and SEM probability maps display gradual changes while the GWR probability map displays clusters and abrupt changes. SLM and SEM have similar frequency histograms with mean values between 0.38 and 0.39 and standard deviations between 0.14 and 0.15. By contrast, GWR shows Leptokurtic distribution with a mean value of 0.51 and a standard deviation of 0.02; SLM and SEM show higher frequencies between 0.40 and 0.50 while GWR shows higher frequencies between 0.45 and 0.55 (Fig. 5, bottom row).

4.2. Simulation and assessment

We calibrated the three CA models to simulate urban pattern at 2005 using ten iterations. Because there is no substantial difference between the results simulated by SLM-CA and SEM-CA, we used SAR-CA to represent these two models. Fig. 6 shows the simulated urban patterns at the 10th iteration that represents the results at 2005. High similarities of overall urban patterns are found between SAR-CA and GWR-CA, and both indicate that the Nanjing urban area expanded outward from the city center to the southeast along the Yangtze River (Fig. 6a-b). The three enlarged areas show apparent differences (Fig. 6c-e), where the enlarged area-1 close to the City center shows that the urban pattern produced by SAR-CA is more compact than that produced by GWR-CA. The enlarged area-2 in the urban fringe area shows a similar phenomenon as in the area-1. The enlarged area-3 in the suburb shows that GWR-CA generated more small urban patches than SAR-CA.

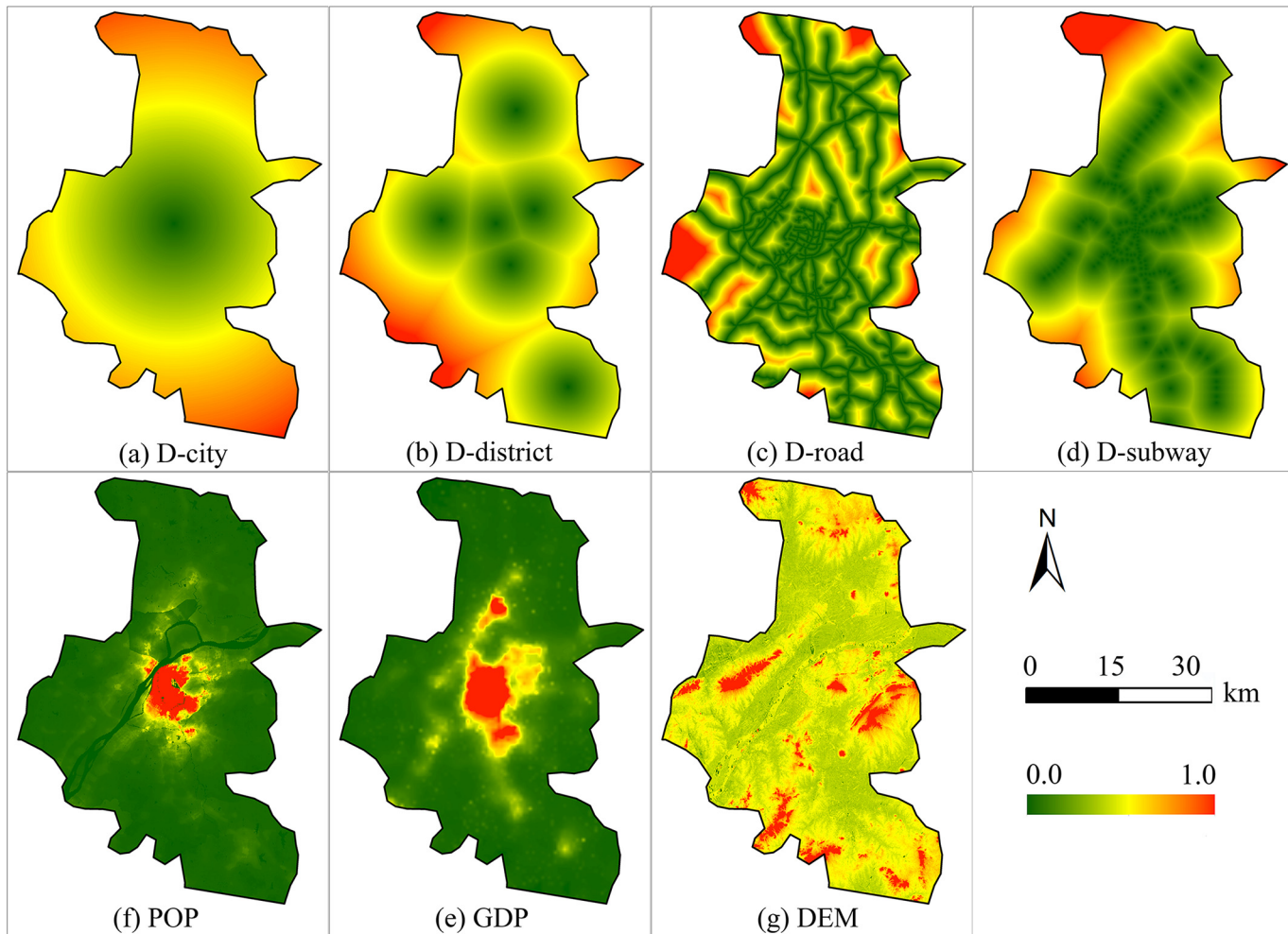


Fig. 4. Proximity, socioeconomic and biophysical variables used in calibrating CA models.

These suggest that GWR-CA can better reflect spatial heterogeneity in urban patterns at Nanjing.

For end-state (urban pattern) assessment, the pixel-by-pixel comparison in 2005 yields OA > 94.0% for both SAR-CA and GWR-CA (Table 4). For all iterations, the end-state assessment by OA shows that SAR-CA is slightly better than GWR-CA, and the differences in OA grow from 0.1% at the 1st iteration to 0.7% at the 10th iteration. The three class-level landscape metrics for urban areas decrease with the model iterations from 1995 to 2005 (Table 4), suggesting decreasing complexity and increasing aggregation of the simulated results. Meanwhile, the sums of the metric differences indicate that SAR-CA has fewer

deviations than GWR-CA in comparison with the real result, indicating better performance of the former in terms of landscape pattern.

For change assessment, we partitioned the urban patterns into initial urban, hits, misses, false alarms, correct rejections, and excluded (Fig. 7a,d), with two sub-areas enlarged to show details (Fig. 7b,e). Substantial differences exist between SAR-CA and GWR-CA, with the former hitting more urban growth (1.6%) than the latter (1.2%). In addition, SAR-CA missed less urban growth in the real map ($-0.4\% = 2.6\%-3.0\%$) and made fewer false alarms ($-0.3\% = 2.5\%-2.8\%$) as compared with GWR-CA (Fig. 7c,f). FOM shows that SAR-CA significantly outperformed GWR-CA in simulating

Table 3
CA transition rule coefficients for the SAR-CA and GWR-CA models.

Variable	SAR-CA				GWR-CA			
	SLM		SEM		Min	Lower Quartile	Mean	Upper Quartile
	Parameter	Rank	Coefficient	Rank				
SAR coefficient	0.29 (ρ)		0.29 (λ)					
Constant	0.07		0.10					
D-city	-0.08	3	-0.11	2	-15.13	-0.08	-0.08	0.12
D-district	-0.06	4	-0.08	4	-61.55	-0.21	0.37	0.51
D-road	0.08	6	0.10	6	-35.24	-0.27	-0.10	0.36
D-subway	0.02	5	0.02	5	-4.24	-0.07	0.03	0.07
POP	-0.16	7	-0.17	7	-15.73	-0.48	-0.19	0.02
GDP	0.17	1	0.19	1	-75.89	-0.31	-0.45	0.72
Elevation	-0.10	2	-0.11	3	-68.68	0.00	0.64	1.12
					-12.79	-0.15	-0.13	0.00

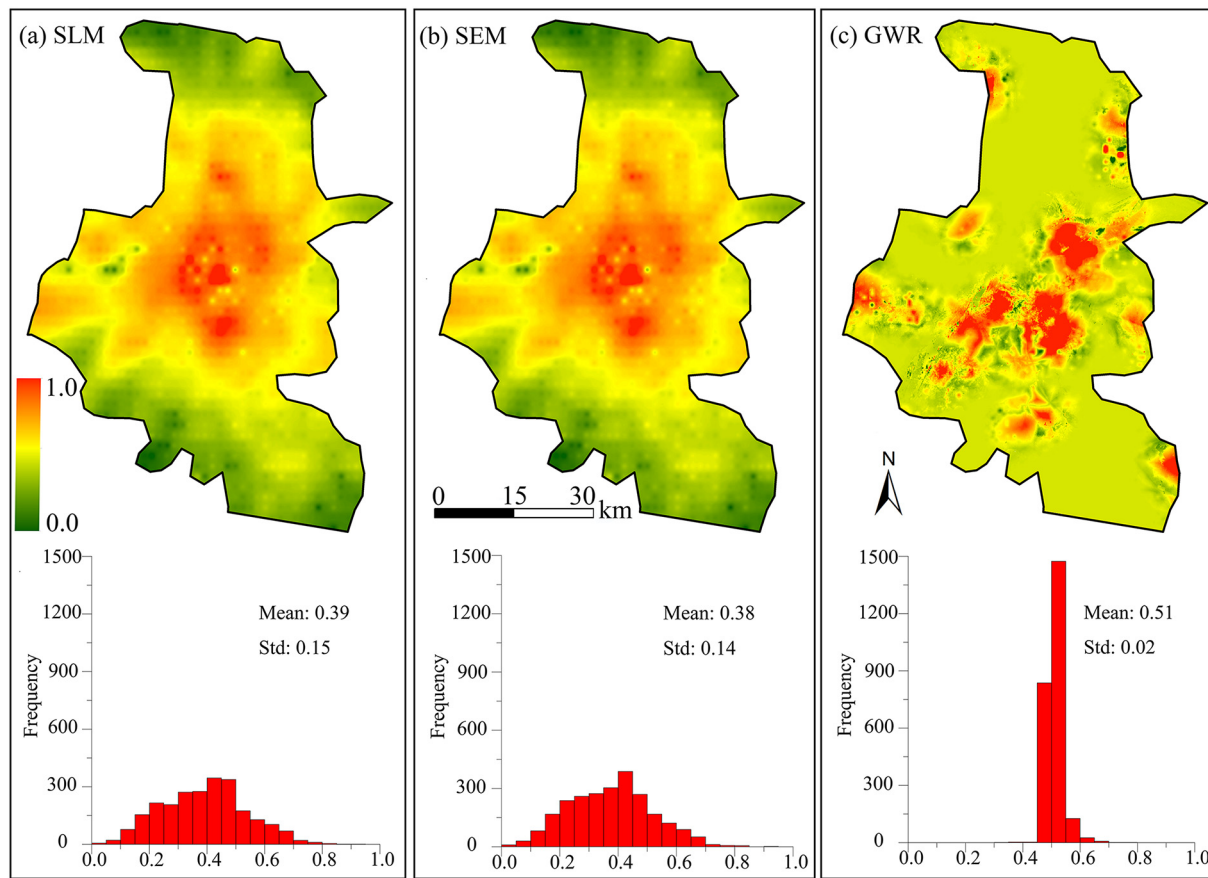


Fig. 5. The three global transition probability maps and their summary statistics.

1995–2005 urban growth by 6.8% ($= 23.9\%-17.1\%$). There are slightly more hits and more false alarms in the enlarged central area for SAR-CA, but slightly more hits and more false alarms in the enlarged suburban area for GWR-CA. The misses show no substantial differences between these two models. Overall, FOM shows that SAR-CA significantly outperforms GWR-CA by 6.8% in reproducing urban growth.

4.3. Validation and prediction

We predicted the 2015 urban patterns using these models for validating their effectiveness. Fig. 8a-b shows the urban extent significantly expanded compared with the earlier decade. The SAR-CA urban pattern shows that the new urban cells are highly concentrated in the City center and its surrounding areas, and there are only a few new urban cells in other areas. For example, the two simulations show significant differences at the north of the Yangtze River (i.e. urban fringe), where more urban cells are found for SAR-CA than for GWR-CA. Also, GWR-CA generated a less clustered pattern in the City center and the urban fringe area (Fig. 8c-d), but produced bigger urban patches in the suburbs (Fig. 8e). These confirm the ability of GWR-CA to model spatial heterogeneity, especially in the suburban areas.

For the validation phase, the 2015 predictions show a decreasing tendency in OA across the model iterations, and the OAs in 2015 are lower than those in 2005. SAR-CA is slightly better than GWR-CA in the prediction at each iteration step, where the OA of the former is slightly higher than that of the latter (Table 5). The greatest OA difference between SAR-CA and GWR-CA (1.5%) occurs on the 10th iteration. The landscape metrics decrease from 2005 to 2015 (Table 4), suggesting that the simulations have reduced complexity and increased aggregation with the model iterations. The sums of the metric differences indicate that SAR-CA has more deviations than GWR-CA in terms of NP

while the former has fewer deviations than the latter in terms of ED and PAFRAC, indicating slightly better performance of the former regarding landscape pattern.

We overlaid the 2005 real map, the 2015 real map, and the 2015 prediction map to examine the two models' ability to predict change (Fig. 9a,d). By comparison, SAR-CA shows more hits and more false alarms but less misses in the enlarged central area, while GWR-CA shows more hits and more false alarms in the enlarged suburban area (Fig. 9b,e). SAR-CA has more polygon-shaped "hit" patches with larger areas while GWR-CA has more edge-shaped "hit" patches with smaller areas. To the south of Nanjing, SAR-CA has more misses with larger patches than GWR-CA. The overlay maps show that SAR-CA hits more urban growth by 0.9% (3.4% - 2.5%) than GWR-CA, and the former has smaller misses and false alarms by -0.9% (6.3% - 7.2%). Ultimately, SAR-CA has led to much higher FOM by 6.2% (21.2% - 15.0%), suggesting its favorable ability to predict urban growth from 2005 to 2015 in terms of the cell-by-cell match.

4.4. Discussion

Machine learning approaches (e.g. GA and PSO) are widely applied in CA modeling for multi-objective urban simulations (Feng & Tong, 2019b; Mustafa, Ebaid, & Teller, 2018), but they have limitations in adequately addressing spatial heterogeneity in urban growth because their CA parameters are spatially stationary (Feng & Tong, 2018; Mirbagheri & Alimohammadi, 2017). In contrast, spatial regression methods have inherent advantages in capturing landscape heterogeneity. We have constructed three CA models based on SLM, SEM and GWR, where the first two yielded highly similar transition probability maps. We calibrated three CA models using these methods at Nanjing from 1995 to 2005. The SAR-CA (e.g. SLM-CA and SEM-CA) and GWR-

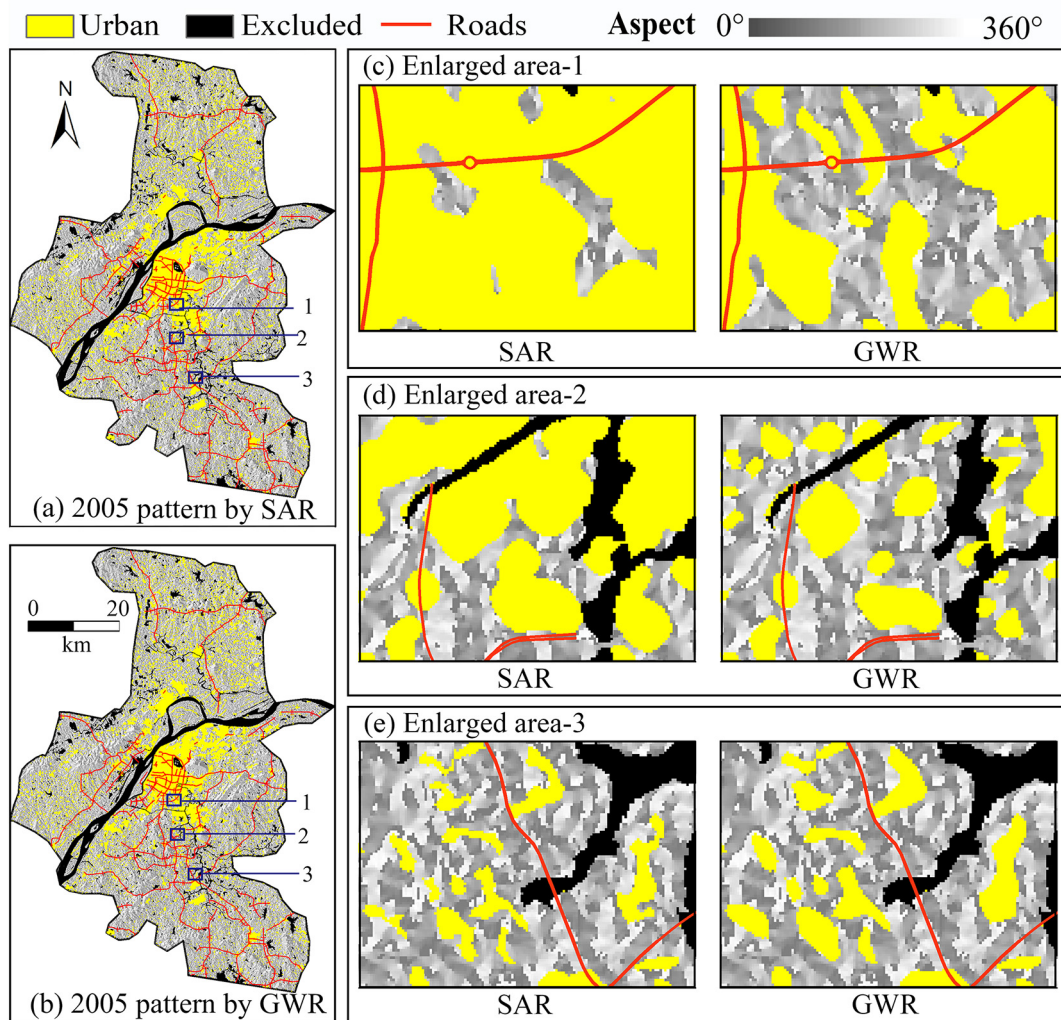


Fig. 6. The simulated urban patterns at 2005 with three enlarged areas to show the details.

CA models were applied to simulate and predict Nanjing's urban growth. Our results show that SAR-CA is superior in assessing both end-state and change, while GWR-CA has advantages of being able to

capture small urban patches buried within suburban areas.

For both calibration and validation, the end-state OAs of both SAR-CA and GWR-CA are high, with the former slightly better than the

Table 4

The end-state assessment of the two models from 1995 to 2005 for ten iterations.

Model	Metric	1995–2005 (%)										Sum of absolute values
		1st	2nd	3rd	4th	5th	6th	7th	8th	9th	10th	
SAR-CA	OA	95.7	95.6	95.6	95.5	95.4	95.3	95.2	95.1	94.9	94.8	5077
	NP	5394	5358	5323	5280	5238	5195	5165	5133	5106	5077	
	ED	19.616	19.417	19.259	19.118	18.985	18.848	18.718	18.593	18.474	18.361	
	PAFRAC	1.283	1.275	1.269	1.264	1.261	1.260	1.257	1.255	1.252	1.249	
GWR-CA	OA	95.6	95.4	95.3	95.2	95.2	95.1	95.0	94.7	94.4	94.1	5087
	NP	5395	5373	5341	5310	5285	5266	5231	5187	5139	5087	
	ED	19.388	19.021	18.798	18.631	18.494	18.381	18.271	18.087	17.903	17.751	
	PAFRAC	1.272	1.254	1.242	1.233	1.224	1.217	1.211	1.198	1.188	1.178	
SAR minus GWR	OA	0.1	0.2	0.3	0.3	0.2	0.2	0.2	0.4	0.5	0.7	
Real minus SAR	NP	-300	-264	-229	-186	-144	-101	-71	-39	-12	17	1363
	ED	1.100	1.299	1.456	1.598	1.731	1.867	1.997	2.122	2.241	2.354	17.765
	PAFRAC	0.031	0.039	0.044	0.049	0.052	0.053	0.057	0.059	0.061	0.064	0.509
Real minus GWR	NP	-301	-279	-247	-216	-191	-172	-137	-93	-45	7	1688
	ED	1.328	1.694	1.918	2.085	2.222	2.335	2.444	2.628	2.813	2.964	22.431
	PAFRAC	0.041	0.060	0.072	0.081	0.090	0.097	0.102	0.115	0.126	0.136	0.920

Note: All three landscape metrics, i.e. NP, ED and PAFRAC, are calculated at the class level for urban area only. NP denotes the number of urban patches to reflect the landscape aggregation, ED (m per ha) denotes the edge density to reflect the amount of urban edges, and PAFRAC denotes a fractal dimension to reflect the urban shape complexity across spatial scales.

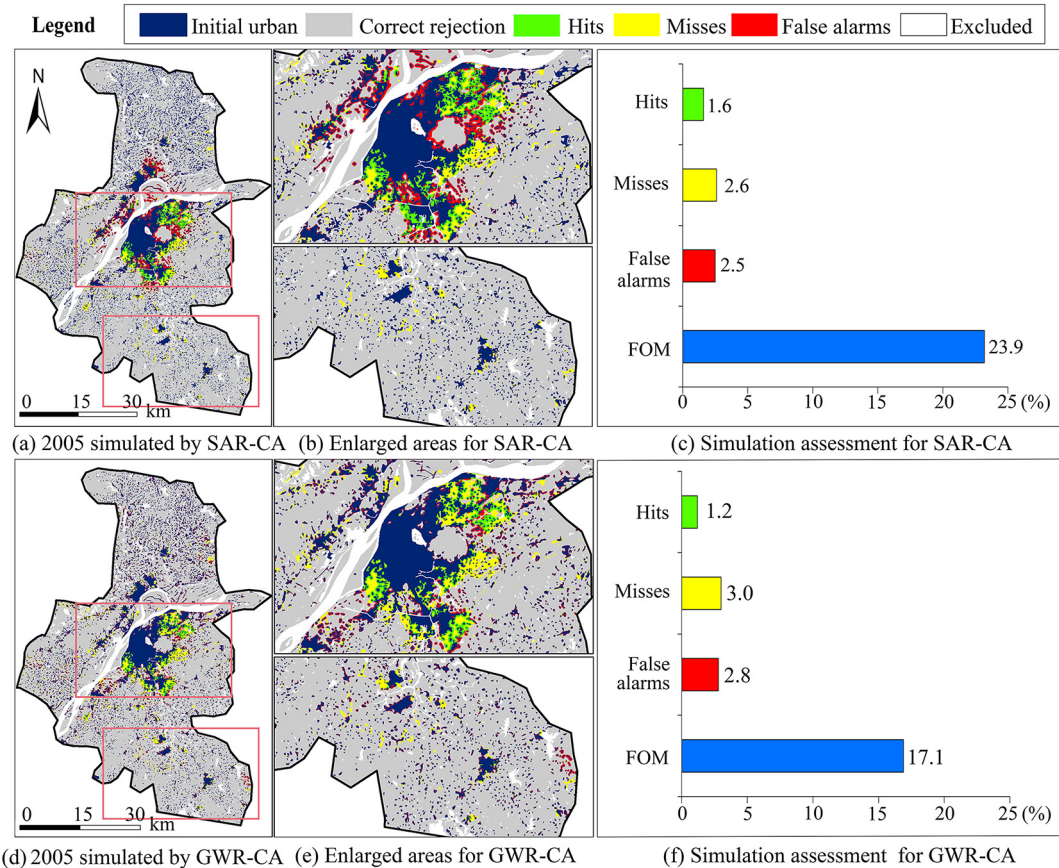


Fig. 7. Partition of the simulation success and error (left) and their statistics (right).

latter. However, high OA does not necessarily denote better modeling ability because it measures only the conformity between the simulated and the real urban patterns (van Vliet et al., 2011). FOM compensates for the disadvantage of end-state accuracy because it is able to explore how the models capture the urban growth (Tong & Feng, 2019b). The OAs of both models are mainly attributable to persistent non-urban areas that are much larger in the earlier steps of the model iteration. This explains why OAs in the calibration phase (1995–2005) are larger than those at the validation phase (2005–2015). In contrast, FOM focuses on the change and indicates the models' ability to capture urban growth. FOM indicates much better performance of SAR-CA as compared to GWR-CA. We found that OA decreases but FOM increases over time (Tables 4& 5 and Figs. 7& 9). We therefore recommend using FOM to evaluate CA models in future studies.

An advantage of SAR and GWR is the ability to delineate spatial heterogeneity in spatially nonstationary transition rules for modeling urban growth. SAR uses implicit methods to reflect spatial heterogeneity by weighting the dependent variable that denotes urban growth (Feng & Tong, 2019a), and considers the spatial autocorrelation when constructing CA transition rules (Feng et al., 2018; Ku, 2016). In contrast, GWR considers the position when fitting the samples and generates a different parameter at each position for each driver (Feng & Tong, 2018; Mirbagheri & Alimohammadi, 2017). Consequently, the parameters of each driver may be positive at one position but negative at another, indicating driver's opposing effects as both accelerating and suppressing urban growth. The buffer-based assessment shows that OA valleys (Fig. 10a-b) correspond to FOM peaks (Fig. 10c-d), where rapid urban growth was found in the regions starting with the critical circles. The area with active urban development was larger during 2005–2015 than during 1995–2005, where the first period has a radius of ~11 km (average of 11 km and 12 km) and the second period has a radius of ~18 km (average of 15 km and 21 km). The 2005 simulation and the

2015 prediction both show that SAR-CA captured more urban growth in the rapidly urbanizing area (left side of the critical triangles) while GWR-CA captured more urban growth in the suburbs (right side of the critical triangles). This suggests that GWR-CA possesses superior ability to reflect spatial heterogeneity in most areas.

Another difference among SLM, SEM and GWR lies in their transition rules that reflect the urban dynamics. Because SLM and SEM can be categorized into SAR, the CA parameters and the related transition probability maps show only marginal differences. This results in high similarities in the simulated results between these two models. In an early study of CA modeling using SAR, the modelers did not distinguish between spatial lag and spatial error (Ku, 2016). In another study, Feng et al. (2018) used spatial lag to construct CA models of urban growth, but the modelers used SAR to name the model. These studies enrich the urban land use change models using implicitly heterogeneous transition rules.

In GWR-CA modeling, the bandwidth in the spatial kernel function substantially influences the regression performance and hence the transition rule construction (Feng & Tong, 2018; Mirbagheri & Alimohammadi, 2017; Su et al., 2014). AIC is a commonly applied metric to assess the transition rule fitting and to select the optimal bandwidth (Huang, Wu, & Barry, 2010). Instead of using AIC, we applied OA and FOM to identify the optimal bandwidth. We performed 12 duplicate experiments using GWR with bandwidths ranging from 30 m to 1000 m, then found that 50 m yields the highest simulation accuracy. Such experiments use considerable computing time, and each needs more time than SAR under the same hardware conditions. However, GWR has the advantages of being able to visualize the spatial distribution of CA parameters, explicitly showing how spatial heterogeneity affects CA modeling (Feng & Tong, 2019a). Overall, our study shows the advantages and disadvantages of using SAR and GWR to construct CA models of urban growth in rapidly-developing areas. The

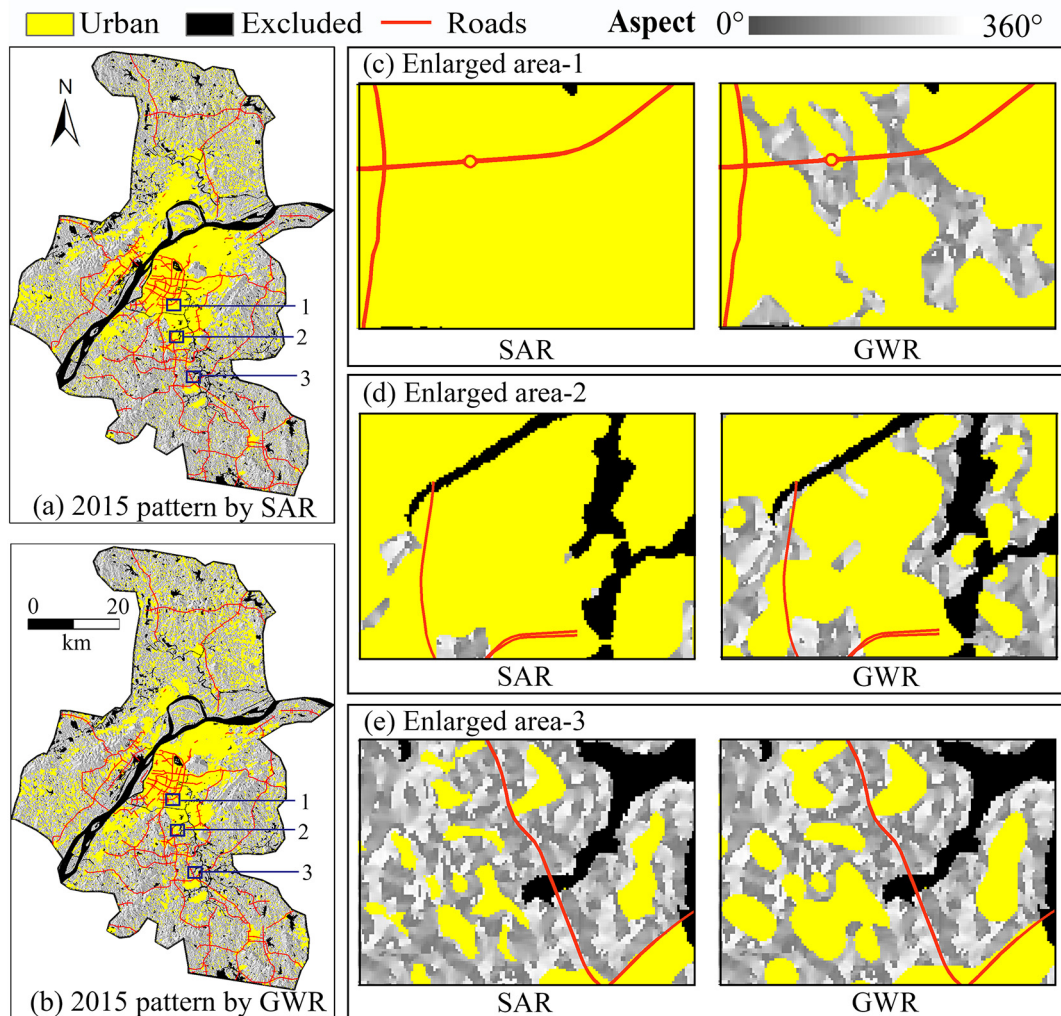


Fig. 8. The simulated urban patterns at 2015 with three enlarged areas to show the details.

comparison of the two types of models should be useful in selecting suitable methods to address spatial heterogeneity in dynamic urban simulation.

Although transition rules and transition probability are central to CA modeling, they are not the only factors affecting the simulation results, because CA models are also influenced by the configuration and

scaling behavior of neighborhood as well as the scaling behavior of transition probability (Dahal & Chow, 2015; Feng & Tong, 2018). Spatial heterogeneity can also be incorporated into the neighborhood effect. The spatially heterogeneous neighborhood is somewhat similar to SAR because both consider the weight of the dependent variable (i.e. urban land use change) and both aim to capture possible heterogeneous

Table 5
The end-state assessment of the two models from 2005 to 2015 for ten iterations.

Model	Metric	2005–2015 (%)										Sum of absolute values
		1st	2nd	3rd	4th	5th	6th	7th	8th	9th	10th	
SAR-CA	OA	90.2	90.0	89.8	89.6	89.3	89.0	88.7	88.3	87.9	87.4	4055
	NP	5010	4909	4813	4728	4650	4566	4468	4405	4323	4243	
	ED	19.751	19.336	19.007	18.769	18.555	18.370	18.206	18.071	17.946	17.820	
	PAFRAC	1.275	1.259	1.243	1.234	1.225	1.220	1.219	1.213	1.211	1.209	
GWR-CA	OA	89.9	89.6	89.3	88.9	88.4	87.9	87.4	87.0	86.5	85.9	32.839
	NP	4985	4890	4819	4740	4673	4541	4413	4295	4174	4059	
	ED	19.410	18.881	18.518	18.220	17.966	17.716	17.506	17.343	17.192	17.166	
	PAFRAC	1.269	1.248	1.228	1.212	1.199	1.187	1.180	1.172	1.165	1.159	
SAR minus GWR	OA	0.3	0.4	0.5	0.7	0.9	1.1	1.3	1.3	1.4	1.5	1.562
	NP	-804	-703	-607	-522	-444	-360	-262	-199	-117	-37	
	ED	2.116	2.531	2.860	3.098	3.312	3.497	3.661	3.796	3.921	4.047	
	PAFRAC	0.112	0.128	0.144	0.153	0.162	0.167	0.168	0.174	0.176	0.178	
Real minus SAR	NP	-779	-684	-613	-534	-467	-335	-207	-89	32	147	3887
	ED	2.457	2.986	3.349	3.647	3.901	4.151	4.361	4.524	4.675	4.701	38.752
	PAFRAC	0.118	0.140	0.159	0.175	0.188	0.201	0.207	0.215	0.222	0.228	1.853

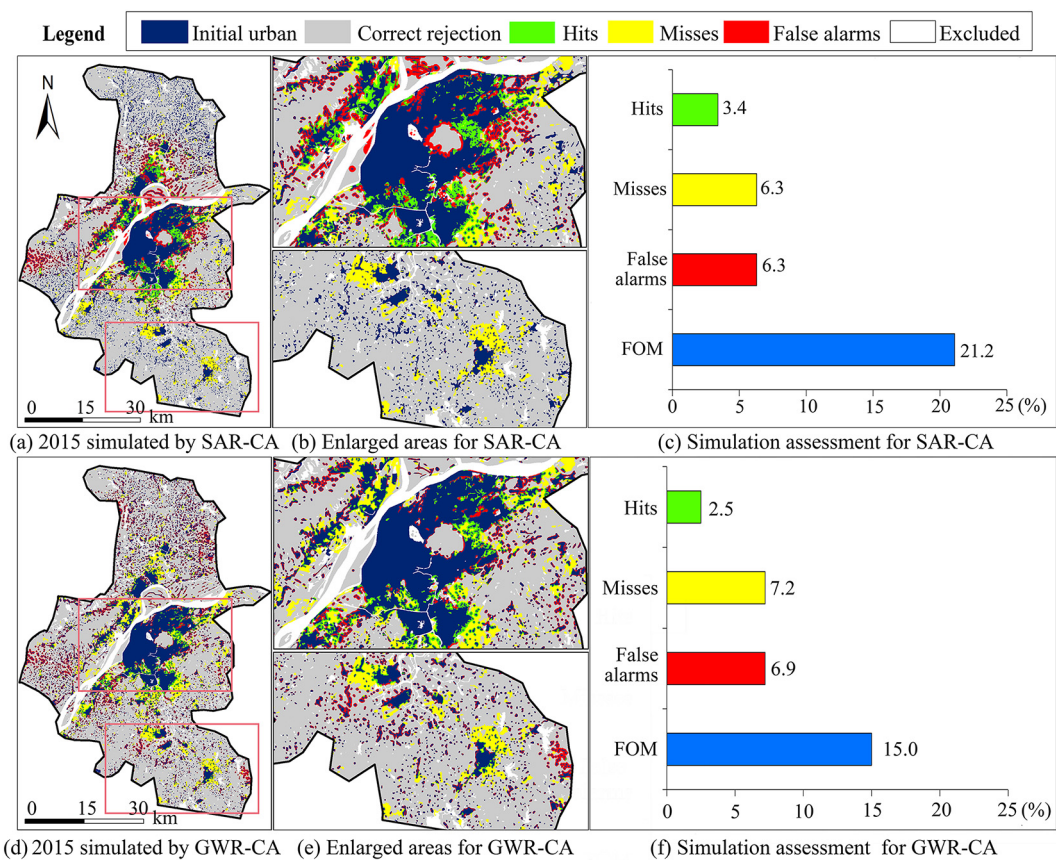


Fig. 9. Partition of the prediction success and error (left) and their statistics (right).

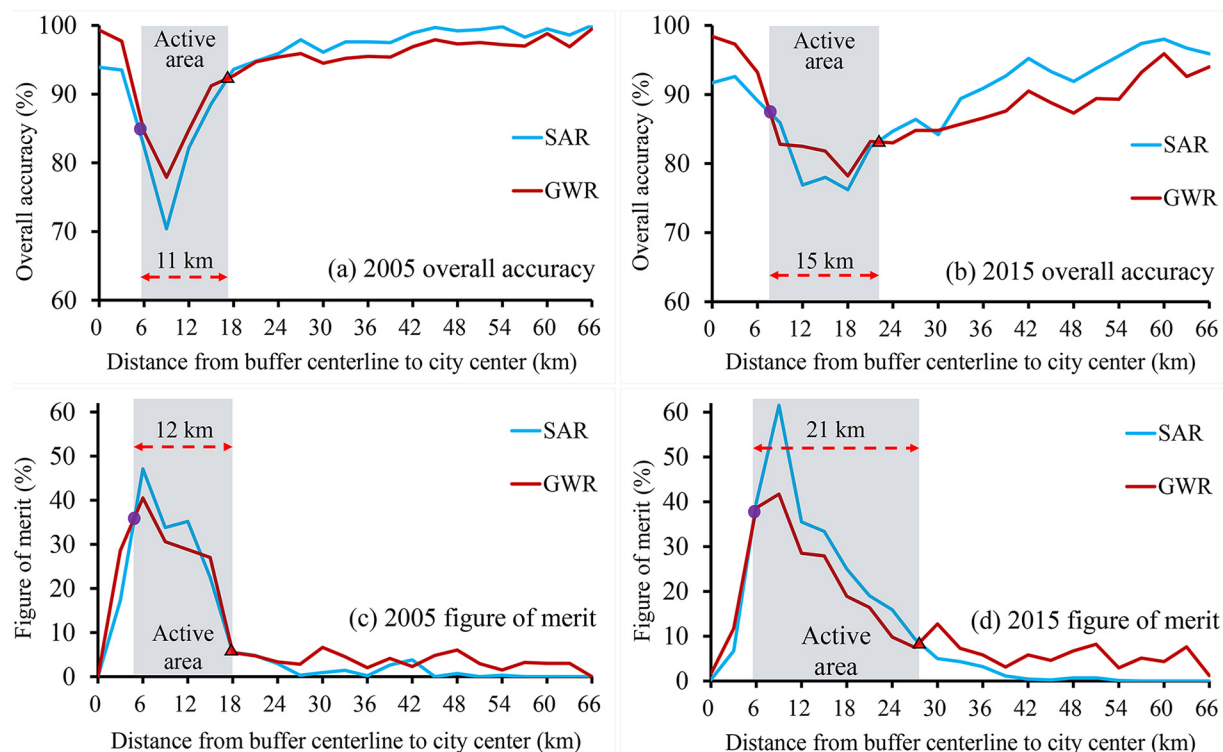


Fig. 10. Comparison of SAR-CA and GWR-CA using a concentric ring buffer-based accuracy assessment.

interactions among neighbors (Feng and Tong, 2019a). The major difference is that spatial regression applies spatially varying parameters to define CA transition rules while heterogeneous neighborhood uses spatially varying neighboring effects. Further work should compare heterogeneous neighborhood and heterogeneous transition rules to suggest the optimal CA modeling approach. In varying degrees, SAR-CA and GWR-CA are sensitive to the spatial scale, randomness factor, neighborhood configuration, threshold selection and CA parameterization, which should be examined in future work.

5. Conclusions

Spatial heterogeneity is inherent to geographic phenomena, and its delineation should help capture the spatially varying relationships between urban growth and its drivers. We compared three local regression methods (SLM, SEM and GWR) in constructing CA models of dynamic urban simulation in Nanjing from 1995 to 2015. SLM and SEM (categorized as SAR) implicitly reflect the nonstationarity of transition rules by incorporating spatial autocorrelation, and these two methods yielded only very marginal differences in the land transition probability and urban patterns. In contrast, GWR explicitly reflects the nonstationarity of transition rules by utilizing position-based CA parameters. The SAR-CA and GWR-CA models well simulated urban growth in Nanjing at the calibration (OA > 94%) and validation (OA > 85%) phases. SAR-CA shows advantages over GWR-CA in simulating urban growth at Nanjing at both phases in terms of OA and FOM; GWR-CA better captures new urban cells in the suburbs (accounting for > 70% of Nanjing), as a consequence better reflecting spatial heterogeneity in urban growth. We recommend using SAR-CA when studying cities with large-scale clustered urban patches (e.g. monocentric pattern and transport-oriented pattern), and examples of such cities are Zhengzhou and Lanzhou in China; in contrast, we recommend using GWR-CA when study cities with many dispersed urban patches (e.g. multicentric pattern), and examples of such cities are Jiaxing and Nantong in China.

Our study presents spatial statistical methods that accurately simulate and predict dynamic urban growth by implicitly and explicitly addressing spatial heterogeneity. It illustrates the pros and cons of SAR and GWR in constructing CA models, and may serve as a reference to describe spatial heterogeneity in urban growth. Spatial heterogeneity can also be incorporated into the CA neighborhood to address locally varying impacts. Future work should compare the effects of spatial regression and heterogeneous neighborhood on the modeling of geographic phenomena, and examine the models' sensitivity related to scale, randomness, neighborhood, threshold, and parameterization.

Acknowledgements

This work was supported by the National Key R&D Program of China (2018YFB0505400 and 2018YFB0505000), the National Natural Science Foundation of China (41771414, 41631178 and 41601414), and the State Key Laboratory of Disaster Reduction in Civil Engineering (SLDRCE19-B-35).

References

- Abdullahi, S., & Pradhan, B. (2018). Land use change modeling and the effect of compact city paradigms: Integration of GIS-based cellular automata and weights-of-evidence techniques. *Environmental Earth Sciences*, 77, 251.
- Alexandridis, A., Russo, L., Vakalis, D., Bafas, G., & Siettos, C. (2011). Wildland fire spread modelling using cellular automata: Evolution in large-scale spatially heterogeneous environments under fire suppression tactics. *International Journal of Wildland Fire*, 20, 633–647.
- Anselin, L. (2016). Spatial externalities, spatial multipliers, and spatial econometrics. *International Regional Science Review*, 26, 153–166.
- Arsanjani, J. J., Helbich, M., Kainz, W., & Boloorani, A. D. (2013). Integration of logistic regression, Markov chain and cellular automata models to simulate urban expansion. *International Journal of Applied Earth Observation and Geoinformation*, 21, 265–275.
- Batty, M., Xie, Y., & Sun, Z. (1999). Modeling urban dynamics through GIS-based cellular automata. *Computers, Environment and Urban Systems*, 23, 205–233.
- Cao, M., Bennett, S. J., Shen, Q., & Xu, R. (2016). A bat-inspired approach to define transition rules for a cellular automaton model used to simulate urban expansion. *International Journal of Geographical Information Science*, 1–19.
- Clarke, K. C. (2018). Cellular automata and agent-based models. *Handbook of regional science* (pp. 1–16). .
- Conway, D., Li, C. Q., Wolch, J., Kahle, C., & Jerrett, M. (2008). A spatial autocorrelation approach for examining the effects of urban greenspace on residential property values. *The Journal of Real Estate Finance and Economics*, 41, 150–169.
- Couclelis, H. (1997). From cellular automata to urban models: New principles for model development and implementation. *Environment and Planning B, Planning & Design*, 24, 165–174.
- Dahal, K. R., & Chow, T. E. (2015). Characterization of neighborhood sensitivity of an irregular cellular automata model of urban growth. *International Journal of Geographical Information Science*, 29, 475–497.
- Debonne, N., van Vliet, J., Heinemann, A., & Verburg, P. (2018). Representing large-scale land acquisitions in land use change scenarios for the Lao PDR. *Regional Environmental Change*, 1–13.
- Dong, J., Dai, W., Shao, G., & Xu, J. (2015). Ecological network construction based on minimum cumulative resistance for the City of Nanjing, China. *ISPRS International Journal of Geo-Information*, 4, 2045–2060.
- Dragičević, S. (2010). Modeling the dynamics of complex spatial systems using GIS, cellular automata and fuzzy sets applied to invasive plant species propagation. *Geography Compass*, 4, 599–615.
- Elhorst, J. P. (2010). Applied spatial econometrics: Raising the Bar. *Spatial Economic Analysis*, 5, 9–28.
- Feng, Y., & Tong, X. (2018). Dynamic land use change simulation using cellular automata with spatially nonstationary transition rules. *GIScience & Remote Sensing*, 55, 678–698.
- Feng, Y., & Tong, X. (2019a). Incorporation of spatial heterogeneity-weighted neighborhood into cellular automata for dynamic urban growth simulation. *GIScience & Remote Sensing*, 1–22.
- Feng, Y., & Tong, X. (2019b). A new cellular automata framework of urban growth modeling by incorporating statistical and heuristic methods. *International Journal of Geographical Information Science*, 1–24.
- Feng, Y., Yang, Q., Hong, Z., & Cui, L. (2018). Modelling coastal land use change by incorporating spatial autocorrelation into cellular automata models. *Geocarto International*, 33, 470–488.
- Fung, T., & Le Drew, E. (1988). The determination of optimal threshold levels for change detection using various accuracy indices. *Photogrammetric Engineering and Remote Sensing*, 54, 1449–1454.
- Gao, J., & Li, S. (2011). Detecting spatially non-stationary and scale-dependent relationships between urban landscape fragmentation and related factors using geographically weighted regression. *Applied Geography*, 31, 292–302.
- Gao, Y., Zhang, C., He, Q., & Liu, Y. (2017). Urban ecological security simulation and prediction using an improved cellular automata (CA) approach—a case study for the City of Wuhan in China. *International Journal of Environmental Research and Public Health*, 14.
- Gashaw, T., Tulu, T., Argaw, M., & Worqlul, A. W. (2018). Modeling the hydrological impacts of land use/land cover changes in the Andassa watershed, Blue Nile Basin, Ethiopia. *Science of the Total Environment*, 619, 1394–1408.
- Gholizadeh, S. (2013). Layout optimization of truss structures by hybridizing cellular automata and particle swarm optimization. *Computers & Structures*, 125, 86–99.
- Guan, Q., Shi, X., Huang, M., & Lai, C. (2016). A hybrid parallel cellular automata model for urban growth simulation over GPU/CPU heterogeneous architectures. *International Journal of Geographical Information Science*, 30, 494–514.
- Hewitt, R., & Diaz-Pacheco, J. (2017). Stable models for metastable systems? Lessons from sensitivity analysis of a cellular automata urban land use model. *Computers, Environment and Urban Systems*, 62, 113–124.
- Huang, B., Wu, B., & Barry, M. (2010). Geographically and temporally weighted regression for modeling spatio-temporal variation in house prices. *International Journal of Geographical Information Science*, 24, 383–401.
- Huang, L., Li, J., Zhao, D., & Zhu, J. (2008). A fieldwork study on the diurnal changes of urban microclimate in four types of ground cover and urban heat island of Nanjing, China. *Building and Environment*, 43, 7–17.
- Irwin, E. G. (2010). New directions for urban economic models of land use change: Incorporating spatial dynamics and heterogeneity. *Journal of Regional Science*, 50, 65–91.
- Kassawmar, T., Eckert, S., Hurni, K., Zeleke, G., & Hurni, H. (2016). Reducing landscape heterogeneity for improved land use and land cover (LULC) classification across the large and complex Ethiopian highlands. *Geocarto International*, 33, 53–69.
- Kocabas, V., & Dragicevic, S. (2007). Enhancing a GIS cellular automata model of land use change: Bayesian networks, influence diagrams and causality. *Transactions in GIS*, 11, 681–702.
- Ku, C.-A. (2016). Incorporating spatial regression model into cellular automata for simulating land use change. *Applied Geography*, 69, 1–9.
- Lai, T., Dragičević, S., & Schmidt, M. (2013). Integration of multicriteria evaluation and cellular automata methods for landslide simulation modelling. *Geomatics, Natural Hazards and Risk*, 4, 355–375.
- Lambin, E. F., & Meyfroidt, P. (2011). Global land use change, economic globalization, and the looming land scarcity. *Proceedings of the National Academy of Sciences*, 108, 3465–3472.
- Liu, X., Hu, G., Ai, B., Li, X., Tian, G., Chen, Y., & Li, S. (2017). Simulating urban dynamics in China using a gradient cellular automata model based on S-shaped curve evolution characteristics. *International Journal of Geographical Information Science*, 32, 73–101.
- Liu, X., Liang, X., Li, X., Xu, X., Ou, J., Chen, Y., ... Pei, F. (2017). A future land use simulation model (FLUS) for simulating multiple land use scenarios by coupling

- human and natural effects. *Landscape and Urban Planning*, 168, 94–116.
- Lu, B., Yang, W., Ge, Y., & Harris, P. (2018). Improvements to the calibration of a geographically weighted regression with parameter-specific distance metrics and bandwidths. *Computers, Environment and Urban Systems*, 71, 41–57.
- Luo, J., & Wei, Y. H. D. (2009). Modeling spatial variations of urban growth patterns in Chinese cities: The case of Nanjing. *Landscape and Urban Planning*, 91, 51–64.
- Ma, S., He, J., Liu, F., & Yu, Y. (2011). Land-use spatial optimization based on PSO algorithm. *Geo-spatial Information Science*, 14, 54–61.
- Mirbagheri, B., & Alimohammadi, A. (2017). Improving urban cellular automata performance by integrating global and geographically weighted logistic regression models. *Transactions in GIS*, 21, 1280–1297.
- Moreno, N., Wang, F., & Marceau, D. J. (2009). Implementation of a dynamic neighborhood in a land-use vector-based cellular automata model. *Computers, Environment and Urban Systems*, 33, 44–54.
- Mur, J., & Angulo, A. (2006). The spatial Durbin model and the common factor tests. *Spatial Economic Analysis*, 1, 207–226.
- Mustafa, A., Ebaid, A., & Teller, J. (2018). Benefits of a multiple-solution approach in land change models. *Transactions in GIS*, 22, 1484–1497.
- Mustafa, A., Heppenstall, A., Omrani, H., Saadi, I., Cools, M., & Teller, J. (2018). Modelling built-up expansion and densification with multinomial logistic regression, cellular automata and genetic algorithm. *Computers, Environment and Urban Systems*, 67, 147–156.
- Mustafa, A., Rienow, A., Saadi, I., Cools, M., & Teller, J. (2018). Comparing support vector machines with logistic regression for calibrating cellular automata land use change models. *European Journal of Remote Sensing*, 51, 391–401.
- Mustafa, A., Saadi, I., Cools, M., & Teller, J. (2018). A time Monte Carlo method for addressing uncertainty in land-use change models. *International Journal of Geographical Information Science*, 32, 2317–2333.
- Nanjing Municipal Bureau Statistics (2015). *Nanjing statistical yearbook 2014*. Beijing: China Statistics Press.
- Omrani, H., Tayyebi, A., & Pijanowski, B. (2017). Integrating the multi-label land-use concept and cellular automata with the artificial neural network-based land transformation model: An integrated ML-CA-LTM modeling framework. *GIScience & Remote Sensing*, 54, 283–304.
- Pérez-Molina, E., Sliuzas, R., Flacke, J., & Jetten, V. (2017). Developing a cellular automata model of urban growth to inform spatial policy for flood mitigation: A case study in Kampala, Uganda. *Computers, Environment and Urban Systems*, 65, 53–65.
- Phipps, M. J. (2018). From local to global: The lesson of cellular automata. *Individual-based models and approaches in ecology* (pp. 165–187). Chapman and Hall/CRC.
- Pinto, N., Antunes, A. P., & Roca, J. (2017). Applicability and calibration of an irregular cellular automata model for land use change. *Computers, Environment and Urban Systems*, 65, 93–102.
- Pontius, R. G., Boersma, W., Castella, J.-C., Clarke, K., de Nijs, T., Dietzel, C., ... Verburg, P. H. (2008). Comparing the input, output, and validation maps for several models of land change. *The Annals of Regional Science*, 42, 11–37.
- Pontius, R. G., & Millones, M. (2011). Death to kappa: Birth of quantity disagreement and allocation disagreement for accuracy assessment. *International Journal of Remote Sensing*, 32, 4407–4429.
- Qiao, W., Gao, J., Liu, Y., Qin, Y., Lu, C., & Ji, Q. (2017). Evaluation of intensive urban land use based on an artificial neural network model: A case study of Nanjing City, China. *Chinese Geographical Science*, 27, 735–746.
- Rimal, B., Zhang, L., Keshtkar, H., Haack, B., Rijal, S., & Zhang, P. (2018). Land use/land cover dynamics and modeling of urban land expansion by the integration of cellular automata and markov chain. *ISPRS International Journal of Geo-Information*, 7, 154.
- Shafizadeh-Moghadam, H. (2019). Improving spatial accuracy of urban growth simulation models using ensemble forecasting approaches. *Computers, Environment and Urban Systems*, 76, 91–100.
- Shu, B., Bakker, M. M., Zhang, H., Li, Y., Qin, W., & Carsjens, G. J. (2017). Modeling urban expansion by using variable weights logistic cellular automata: A case study of Nanjing, China. *International Journal of Geographical Information Science*, 31, 1314–1333.
- Su, S., Li, D., Hu, Y., Xiao, R., & Zhang, Y. (2014). Spatially non-stationary response of ecosystem service value changes to urbanization in Shanghai, China. *Ecological Indicators*, 45, 332–339.
- Tang, R., Tian, L., Thach, T.-Q., Tsui, T. H., Brauer, M., Lee, M., ... Wong, P. (2018). Integrating travel behavior with land use regression to estimate dynamic air pollution exposure in Hong Kong. *Environment International*, 113, 100–108.
- Tobler, W. R. (1970). A computer movie simulating urban growth in the Detroit region. *Economic Geography*, 46, 234–240.
- Tong, X., & Feng, Y. (2019a). How current and future urban patterns respond to urban planning? An integrated cellular automata modeling approach. *Cities*, 92, 247–260.
- Tong, X., & Feng, Y. (2019b). A review of assessment methods for cellular automata models of land-use change and urban growth. *International Journal of Geographical Information Science*, 3, 1–33.
- Triantakonstantis, D., Mountrakis, G., & Wang, J. (2011). A spatially heterogeneous expert based (SHEB) urban growth model using model regionalization. *Journal of Geographic Information System*, 3, 195–210.
- Valipour, M. (2014). Land use policy and agricultural water management of the previous half of century in Africa. *Applied Water Science*, 5, 367–395.
- Ver Hoef, J. M., Peterson, E. E., Hooten, M. B., Hanks, E. M., & Fortin, M. J. (2018). Spatial autoregressive models for statistical inference from ecological data. *Ecological Monographs*, 88, 36–59.
- Vermeiren, K., Vanmaercke, M., Beckers, J., & Van Rompaey, A. (2016). ASSURE: A model for the simulation of urban expansion and intra-urban social segregation. *International Journal of Geographical Information Science*, 30, 2377–2400.
- van Vliet, J., Bregt, A. K., & Hagen-Zanker, A. (2011). Revisiting kappa to account for change in the accuracy assessment of land-use change models. *Ecological Modelling*, 222, 1367–1375.
- Von Neumann, J., & Burks, A. (1966). Theory of self-reproducing automata. *IEEE Transactions on Neural Networks*, 5, 3–14.
- Wang, S.-H., Zhan, T.-M., Chen, Y., Zhang, Y., Yang, M., Lu, H.-M., ... Phillips, P. (2016). Multiple sclerosis detection based on biorthogonal wavelet transform, RBF kernel principal component analysis, and logistic regression. *IEEE Access*, 4, 7567–7576.
- White, R., & Engelen, G. (1993). Cellular automata and fractal urban form: A cellular modelling approach to the evolution of urban land-use patterns. *Environment and Planning A: Economy and Space*, 25, 1175–1199.
- White, R., & Engelen, G. (1997). Cellular automata as the basis of integrated dynamic regional modelling. *Environment and Planning B, Planning & Design*, 24, 235–246.
- Wu, F. (2002). Calibration of stochastic cellular automata: The application to rural-urban land conversions. *International Journal of Geographical Information Science*, 16, 795–818.
- Wu, H., Li, Z., Clarke, K. C., Shi, W., Fang, L., Lin, A., & Zhou, J. (2019). Examining the sensitivity of spatial scale in cellular automata Markov chain simulation of land use change. *International Journal of Geographical Information Science*, 33, 1040–1061.
- Yi, Y., Kimball, J. S., Chen, R. H., Moghaddam, M., Reichle, R. H., Mishra, U., ... Oechel, W. C. (2018). Characterizing permafrost active layer dynamics and sensitivity to landscape spatial heterogeneity in Alaska. *The Cryosphere*, 12, 145–161.
- Zaitsev, D. A. (2017). A generalized neighborhood for cellular automata. *Theoretical Computer Science*, 666, 21–35.
- Zhang, R., Du, Q., Geng, J., Liu, B., & Huang, Y. (2015). An improved spatial error model for the mass appraisal of commercial real estate based on spatial analysis: Shenzhen as a case study. *Habitat International*, 46, 196–205.
- Zhang, X., Hu, M., Chen, G., & Xu, Y. (2012). Urban rainwater utilization and its role in mitigating urban waterlogging problems—A case study in Nanjing, China. *Water Resources Management*, 26, 3757–3766.
- Zhao, Z., Chen, W., Wu, X., Chen, P. C., & Liu, J. (2017). LSTM network: A deep learning approach for short-term traffic forecast. *IET Intelligent Transport Systems*, 11, 68–75.